Size Statistics of Cumulus Cloud Populations in Large-Eddy Simulations

R. A. J. NEGGERS

Department of Atmospheric Sciences, University of California, Los Angeles, Los Angeles, California

H. J. J. JONKER

Thermofluids Section, Department of Applied Physics, Delft University of Technology, Delft, Netherlands

A. P. SIEBESMA

Royal Netherlands Meteorological Institute, De Bilt, Netherlands

(Manuscript received 29 November 2001, in final form 9 July 2002)

ABSTRACT

Cloud size distributions of shallow cumulus cloud populations are calculated using the large-eddy simulation (LES) approach. A range of different cases is simulated, and the results are compared to observations of real cloud populations. Accordingly, the same algorithm is applied as in observational studies using high-altitude photography or remote sensing.

The cloud size density of the simulated cloud populations is described well by a power law at the smaller sizes. This scaling covers roughly one order of magnitude of cloud sizes, with a power-law exponent of -1.70, which is comparable to exponents found in observational studies. A sensitivity test for the resolution suggests that the scaling continues at sizes smaller than the standard grid spacing. In contrast, on the other end, the scaling region is bounded by a distinct scale break. When the cloud size is nondimensionalized by the scale break size, the cloud size densities of all cases collapse. This corroborates the idea of a universal description for the whole cloud size density, with the scale break size as the only variable. The intermediate dominating size in the cloud fraction and mass flux decompositions is directly related to the presence of the scale break in the cloud size density. Despite their large number, the smallest clouds contribute very little to the total vertical mass transport. The intermediate size of the dominating clouds in the cloud fraction and mass flux is insensitive to the resolution of LES.

1. Introduction

Shallow cumulus cloud fields are inhomogeneous and broken in structure, and the individual clouds are irregular over a wide range of scales. This complicates the parameterization of the radiative and transport effects of such cloud ensembles in general circulation models (GCMs) in several ways. First, such cloud populations scatter incoming solar radiation in all directions. A radiation scheme that has knowledge of the geometrical structure of such a cloud field is required. Second, convection schemes in GCMs are used to predict the vertical transport of heat, moisture, and momentum by convective cloud fields (e.g., Arakawa and Schubert 1974; Tiedtke 1989; Gregory 2001). To describe the interaction between clouds and their environment, entrainment and detrainment rates are used. Many theories exist on the relation between cloud mixing and cloud size. Accordingly, more observational evidence is needed about the cloud size distribution, and about the clouds that contribute most to the cloud fraction and vertical transport.

These issues have been the motivation behind many observational studies of shallow cumulus cloud populations. Such studies have used aircraft photographic images, radar data, satellite images, and other remote sensing instruments. There have been many efforts to extract a functional relation for the *cloud size density*, defined as the probability density function of the number of clouds as a function of cloud size. The goal is to find out if a universal functional form exists that contains a minimum but enough nonuniversal parameters to apply to all situations. However, there is no agreement on this yet. Several possible candidates are mentioned in the literature: an exponential (Plank 1969; Wielicki and Welch 1986), a lognormal (Lopez 1977), and various power laws (Cahalan and Joseph 1989; Kuo et al. 1993; Benner and Curry 1998). The three studies last mentioned report a scale break in the power law, which has

Corresponding author address: R. A. J. Neggers, Department of Atmospheric Sciences, University of California, Los Angeles, Los Angeles, CA 90095-1565.
E-mail: neggers@atmos.ucla.edu

© 2003 American Meteorological Society

Unauthenticated | Downloaded 05/26/24 10:08 PM UTC

been related by Cahalan and Joseph (1989) to the largest individual convective cells that exist in the boundary layer. Nevertheless, Lopez (1977) pointed out that no analysis of observational results has yet been able to exclude any of these candidates for certain.

Concerning the cloud fraction, small cumulus clouds are the most numerous in the population but cover a relatively little area individually. On the other hand, large clouds individually cover a large area but seldom occur. Due to this trade-off between cloud number and cloud size, it is not known a priori what size clouds contribute most to the total cloud fraction of the population. Observational evidence was presented by Plank (1969) using photographs of cumulus cloud fields over Florida taken from aircraft, and by Wielicki and Welch (1986) using Landsat images. In all cases, an intermediate size between the largest and smallest size present in the population dominated the cloud fraction. The dominating size varies over the cumulus scenes studied, but is always well defined and intermediate. Closely related to the cloud area is the vertical mass flux by a cloud, being the product of cloud area and cloud vertical velocity (Arakawa and Schubert 1974; Tiedtke 1989). Knowledge of the vertical velocities inside clouds is required to calculate mass flux distributions. Measurements of both the cloud diameter and the vertical velocity of individual clouds can be provided by aircraft trajectories through cumulus clouds (e.g., Warner 1970, 1977; Raga et al. 1990; Barnes et al. 1996) or radar measurements (e.g., Lehrmitte 1987; Knight and Miller 1998; French et al. 1999; Kollias et al. 2001). However, the number of clouds measured with these methods is typically much smaller than the number captured by satellite images, which complicates the calculation of reliable cloud size densities.

Due to improved supercomputer capacity over the last decades, large-eddy simulation (LES) has become another tool to study boundary layer clouds. The LES concept has several useful advantages that observational data cannot offer. First, it can be used to simulate detailed, time-dependent, full three-dimensional fields of the thermodynamic variables and (vertical) momentum. For example, mass flux distributions as a function of cloud size can be calculated easily in LES. Second, it offers unparalleled statistics because the number and duration of the simulations are limited only by the ever-growing supercomputer capacity. Third, and most important, all conditions of the simulated case are exactly defined and completely controlled by the user, which enables the reproduction of obtained results for similar settings. This makes LES useful for studying the impact of certain key variables that are thought to be relevant in the problem. It is therefore ideal to test hypotheses or parameterizations for GCMs. Several LES intercomparison studies by the Global Energy and Water Cycle Experiment (GEWEX) Cloud Systems Studies working group 1 (GCSS wg1) have shown that LES is robust in reproducing the bulk vertical turbulent transport of the cloud ensemble (Stevens et al. 2001; Brown et al. 2002; Siebesma et al. 2003).

In spite of all these advantages, LES is still a numerical model, and the question remains if LES realistically resolves the individual clouds that are most important for the projected cloud fraction and mass flux. More insight into this problem can be obtained by studying the properties of simulated clouds and comparing them to observations of real clouds. For example, Xu and Randall (2001) compared the updrafts and downdrafts in cumulus clouds as simulated by a cloud-resolving model to aircraft observations. Siebesma and Jonker (2000) showed that the fractal dimension of *individual* cloud boundaries are in excellent agreement with observations (Lovejoy 1982). However, to characterize whole cloud *populations*, cloud size distributions have to be used. One of the earliest attempts to do this in LES is described by Beniston and Sommeria (1981), but then the results were still hampered by a coarse resolution. The most recent study of simulated cloud size distributions using LES was published by Brown (1999b), who evaluated the sensitivity of the cloud size distributions to the numerical resolution.

This study critically compares the cloud size densities produced by LES to those of observed natural cloud fields as reported in the literature. To enable a straightforward comparison, exactly the same method is used in deriving the cloud size densities, and a comparable number of clouds is sampled. Several different shallow cumulus cases are simulated, and the results are used to study the universality of the functional form thought to be applicable to the cloud size density. To this purpose, typical relevant scales are searched in order to reduce the problem of reconstructing the cloud size density to a minimum number of parameters. Furthermore, the underlying relations between the cloud size density and the decompositions of the cloud fraction and mass flux with cloud size are used to investigate which cloud size contributes most to these properties. Finally, some sensitivity tests are performed to study the impact on these results of several numerical features and of the vertical wind shear.

The LES model used in this study and the cumulus cases simulated are described briefly in section 2. The necessary definitions and the method are presented in section 3. The results are given in section 4, and are discussed in section 5.

2. The LES model and case descriptions

A detailed description of the Royal Netherlands Meteorological Institute (KNMI) LES model used in this study is given by Cuijpers and Duynkerke (1993); therefore, only a short description will be given here. The governing equations for high Reynolds number atmospheric flow are applied to a limited three-dimensional domain and filtered at a certain length scale in the inertial subrange of turbulence. The resulting discretized equa-

Unauthenticated | Downloaded 05/26/24 10:08 PM UTC

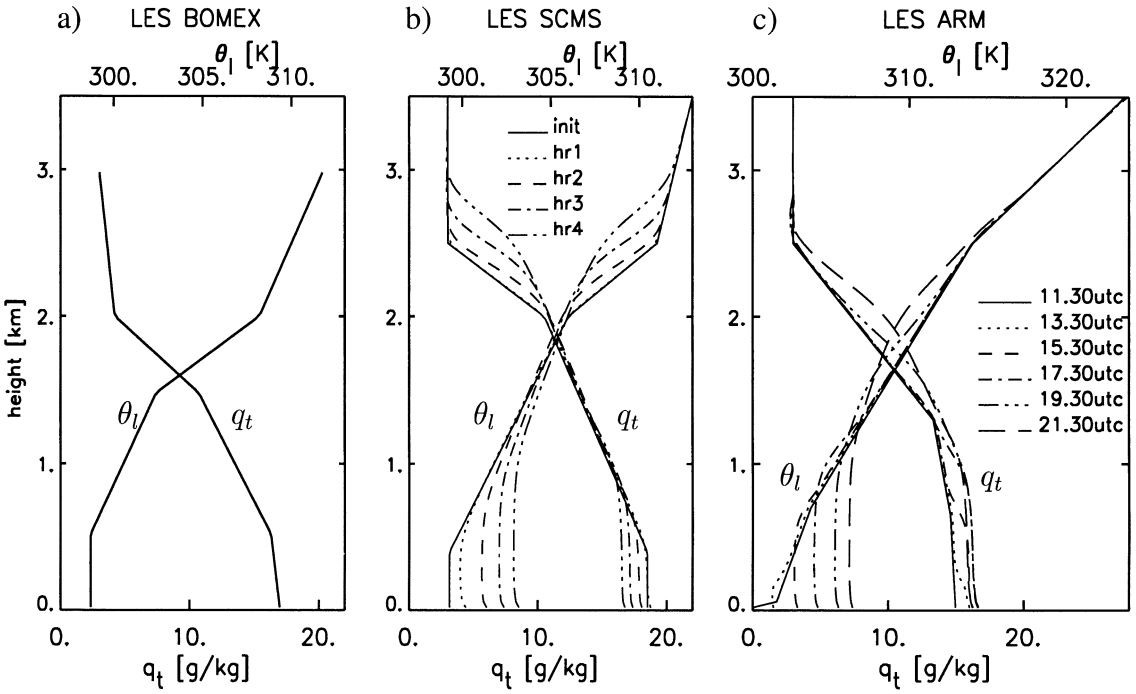

FIG. 1. Overview of the vertical profiles of total specific humidity q_t and liquid water potential temperature θ_l of (a) the BOMEX case, (b) the ARM case, and (c) the SCMS case. The initial profiles are drawn as solid lines, subsequent hourly averages of the LES simulations have a different style as indicated by the legend.

tions are solved using a centered difference advection scheme and time integration is performed. The subgrid model uses a prognostic equation for the turbulent kinetic energy on subgrid scales. The subgrid length scale ℓ_0 is related to the grid spacing, $\ell_0 \sim (\Delta x \Delta y \Delta z)^{1/3}$. Close to the surface ℓ_0 is taken proportional to the height above the surface. The subgrid length scale is also corrected for stable conditions.

Three different shallow cumulus cases are selected for simulation. Each LES case is based on the measurements and observations made during the measurement campaign of the corresponding name. An overview of the vertical profiles of all cases is given in Fig. 1. For the details of the simulations, see Table 1. The first case is based on Barbados Oceanographic and Meteorology Experiment (BOMEX) during which steady-state cumulus convection was observed for a period of several days (Holland and Rasmusson 1973; Nitta and

TABLE 1. Overview of the details of the simulations of all cases. Δ_x, Δ_y, and Δ_z are the grid spacings on the three spatial axes, and L_x, L_y, and L_z are the corresponding dimensions of the simulated domain. Q_H and Q_L stand for the sensible and latent heat flux at the surface. Every 5 min a 3D instantaneous field was sampled for clouds. To obtain sufficient statistics, more than one run was performed, using a differently randomized initial temperature profile.

Case	Grid spacing (m)		Domain size (km)		Surface fluxes (W m^{-2})		No. of sampled clouds
	Δx, Δy	Δz	L_x, L_y	L_z	Q_H	Q_L	
BOMEX							
Reference	50	40	6.4	3			36.776
High resolution	25	″	″	″			25.417
Low resolution	100	″	″	″	8	150	22.652
High shear 2×	50	″	″	″			18.379
No shear 0×	50	″	″	″			20.542
SCMS							
Reference	50	40	6.4	5			20.268
Large domain	100	″	12.8	″	150	300	16.404
Small domain	25	″	3.2	″			18.118
ARM							
Diurnal cycle	66.67	40	6.4	4.4	140 Max at noon	500	35.137 Whole day

Unauthenticated | Downloaded 05/26/24 10:08 PM UTC

Esbensen 1974). A detailed description can be found in Siebesma and Cuijpers (1995). The convection in the boundary layer is driven by surface fluxes, the latent and sensible heat fluxes are 150 and 8 W m^{-2}, respectively. A dry well-mixed layer is topped by a conditionally unstable cloud layer, which in turn is capped by a stable trade wind inversion (see Fig. 1a). A prescribed large-scale subsidence at the inversion causes drying and warming in the LES case, balancing the moistening and cooling effect of the clouds. An ensemble of 10 BOMEX runs is performed, each member initialized with a differently randomized initial temperature profile, which causes the runs to be statistically independent. The first 3 h of each simulation are considered as the startup phase in which the system had to find its steady-state equilibrium. This results in about 4 $\times 10^4$ sampled clouds, which makes the statistical quality of the resulting histograms comparable to observational studies, which are typically based on 10^4 clouds.

The second case is based on observations on 5 August 1995 of the Small Cumulus and Microphysics Study (SCMS). This cloud measurement campaign took place near Cocoa Beach, Florida. On this day, strong cumulus convection was observed over land. The initial profiles are based on flight legs made during the afternoon, during which the temperature and humidity of the cloud-free atmosphere was measured up to 4 km. The cloud layer was about 1.5 km thick and was deepening with time, see Fig. 1b. The surface latent and sensible heat fluxes were set constant in time at 300 and 150 W m^2, respectively. Note that the sensible heat flux is about 20 times larger than that of the BOMEX case. The geostrophic wind forcing was $(-4, 4)$ m s^{-1} in the zonal and meridional direction, and fairly constant with height. The friction velocity at the surface was 0.18 m s^{-1}. The stronger surface fluxes compared to the BOMEX case cause more vigorous vertical transport by the clouds. Consequently, this case is suitable for use in a sensitivity test on the domain size used in LES. When chosen too small, the dimensions of the domain at some stage limit further growth of the maximum cloud size in the spectrum.

Finally, the third case is based on development of shallow cumulus over land such as observed on 21 June 1997 at the Southern Great Plains (SGP) site in Oklahoma of the Atmospheric Radiative Measurement (ARM) program. This case has been designed for an LES intercomparison study of GCSS (Brown et al. 2002). A diurnal cycle was observed in a cumulus-topped convective boundary layer over land. Radiosonde soundings, surface flux measurements, and cloud radar observations were made on this day. This case is initialized at 1130 UTC around sunset with a stable boundary layer (see Figs. 1c and 2). During the morning the surface fluxes increase to a maximum at 1900 UTC, and as a result a dry convective boundary layer develops. Above this layer a conditionally unstable cloud layer forms at about 1430 UTC, which deepens with time. It is interesting to study how the cloud population reacts to the deepening cloud layer and the changing surface fluxes in this case.

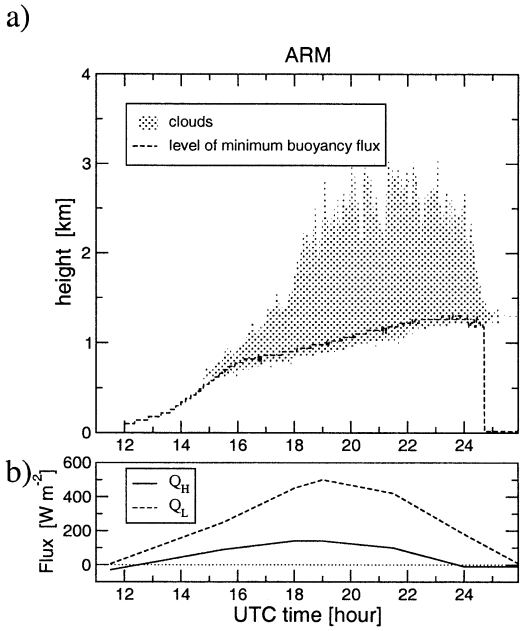

FIG. 2. Time series of (a) the heights of cloud top and cloud base and (b) the surface fluxes during the diurnal cycle of the ARM case. The total heat flux is the sum of the latent and sensible heat fluxes. Local time is UTC minus 6 h. The height of the level of minimum buoyancy flux $z_{w\theta v}$ is also plotted in (a) to indicate the depth of the dry convective boundary layer. At about 0100 UTC the cumulus convection breaks down totally.

Fewer clouds could be sampled in the SCMS and ARM cases compared to BOMEX, because they are not in steady state, and the sampling period per run was therefore kept relatively short.

3. Definitions

The *cloud size distribution* of cumulus cloud populations is defined as the integral over a probability density function (pdf). This pdf, also known as a *cloud size density*, is the probability of occurrence of a cloud of a certain size. Cloud size *decompositions* can be calculated for some important properties that characterize the population, that is, the cloud fraction and the vertical mass flux as a function of cloud size.

An algorithm has to be defined to extract cloud size densities from simulated cloud fields produced by LES. The method of deriving them will be kept as close as possible to those of previous observational studies, in order to be able to compare the LES results to data of real cloud populations. Each cloud (n) in the population is first given a unique linear size (ℓ_n). Although seemingly trivial, this is an important subject as there are many options for the definition of the ''size'' of a cloud (see Fig. 3). The most simple definition is to take the square root of the area of the cross section of a cloud

Unauthenticated | Downloaded 05/26/24 10:08 PM UTC

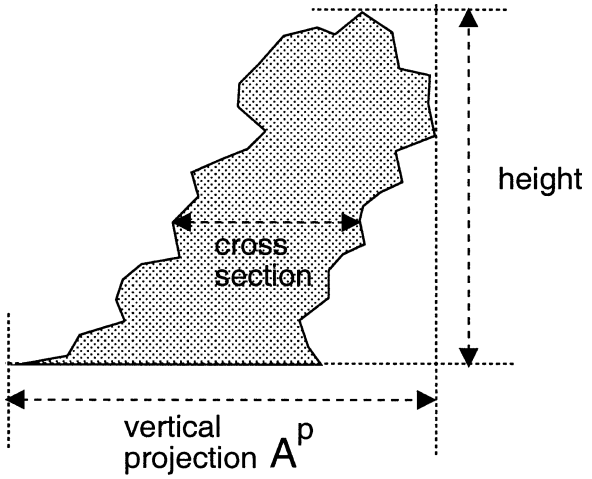

FIG. 3. Several different measures of a single cumulus cloud, shown in a schematic vertical cross section.

at a certain height. But when using two-dimensional (projected) images of real cloud fields taken from high altitudes, the vertically projected area A_n^p of a cloud n has to be used:

$$\ell_n = \sqrt{A_n^p}. \tag{1}$$

As there have been many analyses of satellite images in the past, we want to compare the LES results to these studies and accordingly we prefer to use this definition.

Once the linear size ℓ_n has been defined, we can sort all the clouds by their size and build histograms. This algorithm is described in detail in the appendix, and so only the most important definitions will be mentioned at this point. The total number of clouds N present in the domain at a certain time is defined by the integral of the corresponding cloud size density $\mathcal{N}(l)$:

$$N \equiv \int_0^\infty \mathcal{N}(l)\, dl, \tag{2}$$

where the term $\mathcal{N}(l)$ is the number of clouds of size l in the domain. The *cloud fraction* of a cloud field is defined as the ratio between the area covered by all clouds and the total area of the domain. From vertical projections of real cumulus cloud fields as observed from high altitudes, only the *vertically projected* cloud fraction a^p can be derived, defined as the integral of the cloud fraction decomposition α^p over the cloud size l,

$$a^p \equiv \int_0^\infty \alpha^p(l)\, dl. \tag{3}$$

The cloud fraction decomposition α^p denotes the contribution to a^p as a function of cloud size l, and can be written as

$$\alpha^p(l) \equiv \frac{l^2\, \mathcal{N}(l)}{L_x L_y}, \tag{4}$$

where L_x and L_y are the horizontal dimensions of the domain. This means that once $\mathcal{N}$ is known α^p is also known.

Another property often studied is the cloud fraction *at one height* $a(z)$, defined as the horizontal area covered by clouds at height z divided by the total area of the domain. This can typically be derived from data measured by aircraft flying through cumulus clouds. Evaluating $a(z)$ at different heights using cloud size densities gives information about the most important clouds for the cloud fraction as a function of height. The definition of the height-dependent cloud fraction decomposition $\alpha(l, z)$ is comparable to (4) and (3); the only difference is that $\mathcal{N}$ is now calculated for a number of different height ranges.

The vertical *mass flux* associated with a cloud population is usually defined as the product of the cloud fraction and the cloud-average vertical velocity w,

$$m(z) \equiv a(z)\, w(z). \tag{5}$$

The mass flux decomposition $\mu(l, z)$ at height z is defined as

$$m(z) \equiv \int_0^\infty \mu(l, z)\, dl, \qquad \mu(l, z) \equiv \alpha(l, z)\, w(l, z), \tag{6}$$

where $w(z, l)$ is the average vertical velocity of the clouds of size l at height z. In order to reach a height-independent definition of the mass flux, we introduce an average mass flux over the depth of the cloud layer,

$$m \equiv \int_0^\infty \mu(l)\, dl, \qquad \mu(l) \equiv \frac{1}{h_c} \int_{h_c} \mu(l, z)\, dz, \tag{7}$$

where h_c is the depth of the cloud layer. To prevent a cloud from being represented in different bins at different levels when calculating $\mu(l)$ using (7), the clouds are sorted using the same size at all heights, namely its vertically projected area [see (1)]. In this way, $\mu(l)$ is analogous to $\alpha^p(l)$.

It is likely that $\alpha^p(l)$ differs from $\alpha(l, z)$, as cloud overlap has a significant impact. Brown (1999b) calculated cloud fraction decompositions at one height in BOMEX using LES. In contrast, we will concentrate on the vertically projected fields to enable a straightforward comparison to satellite data.

4. Results

In order to critically compare the cloud populations produced by LES to high-resolution observations of real cloud populations, the cloud size densities need to be characterized by fitting one of the functions proposed in the literature. Subsequently, the resulting parameters can be compared to the observed values.

As mentioned in the introduction, there have been many efforts to extract a functional relation for the cloud size density from observations of natural cloud populations, but there is no agreement on this yet. An early

Unauthenticated | Downloaded 05/26/24 10:08 PM UTC

proposed functional form is the exponential (Plank 1969; Wielicki and Welch 1986). Lopez (1977) suggested the lognormal function. The most frequently mentioned proposition in recent years is the power law (e.g., Cahalan and Joseph 1989; Kuo et al. 1993; Benner and Curry 1998). Accordingly, to the purpose of a comparison of LES results with recent observations as quantitatively as possible, we also use the power-law functional form, defined by

$$\mathcal{N}(l) = a\, l^b. \tag{8}$$

A scale break is defined as the cloud size at which this functional relation breaks down or, in other words, the size where the exponent b suddenly changes. The match between LES and observations in terms of the parameters resulting from power-law fits on the densities is a good indication of how realistic the simulated cloud populations actually are.

All histograms presented in this section were obtained by sorting in equidistant bins on a linear ℓ axis. However, the cloud size density $\mathcal{N}$ is normally plotted using log–log axes for better visualization. The relationship between the histogram $\mathcal{N}$ on a linear and on a logarithmic l axis is given by

$$\mathcal{N}^*(\log l) = \mathcal{N}(l)\frac{dl}{d\,\log l} = l\,\ln 10\,\mathcal{N}(l). \tag{9}$$

Note that if $\mathcal{N}(l)$ is a power law, $\mathcal{N}^*(\log l)$ is also a power law but with the exponent increased by 1.

a. Cloud size densities

Figure 4a shows the histogram of the cloud size density $\mathcal{N}^*$ for the simulated cases based on ARM, BOMEX, and SCMS. Each case is simulated using the same domain size and approximately the same resolution. Here $\mathcal{N}^*$ is normalized by the total number of clouds (N) in the domain. What immediately catches the eye is the collapse of the three histograms for the smaller clouds. In all cases the slope of the density is approximately constant in a range of sizes of more than one order of magnitude wide. This suggests that in this region the density is well represented by a power-law function with a negative exponent. The other functional forms are less likely to apply in this region, as both lognormal (Lopez 1977) and exponential (Wielicki and Welch 1986) functions have nonconstant derivatives and intermediate maxima in a log–log plot.

Accordingly, a linear least squares fit is applied to the scaling range of sizes bounded by the grid spacing on one end and a distinct scale break on the other (see Fig. 4a). The slope of the density is -0.70, somewhat larger than the value of -0.89 found by Cahalan and Joseph (1989) for remote sensed real clouds. The value of -0.70 corresponds by formula (9) to $b = -1.70$ in (8). Benner and Curry (1998) calculated power-law exponents of many tropical shallow cumulus cloud populations, and found it to be on average -1.98 for the smaller clouds, with some spread around this value. Therefore, considering both the value of the power-law exponent at the smaller sizes and the presence of a scale break, these simulated cloud populations using LES seem realistic. Figure 4b further emphasizes the robustness of the typical slope of the cloud size density below the scale break in LES.

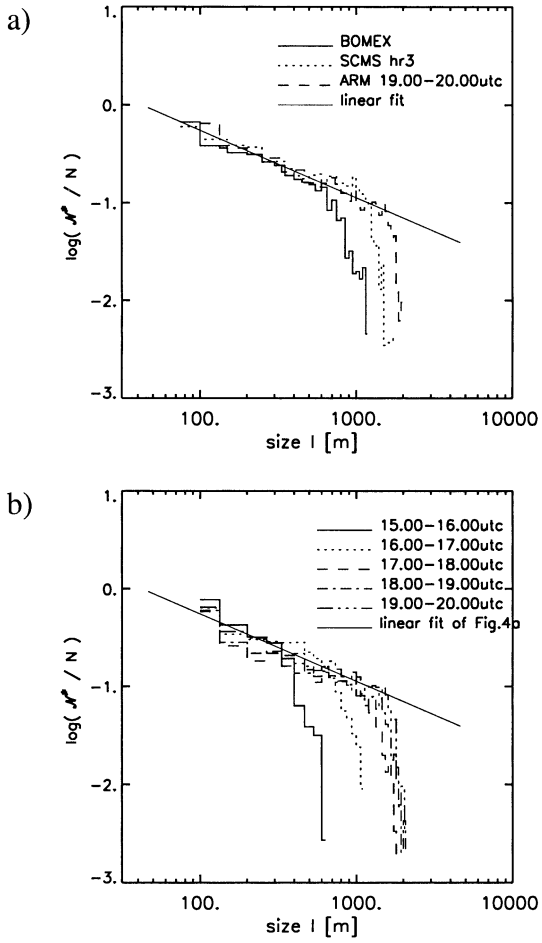

FIG. 4. The normalized cloud size density $\mathcal{N}^*/N$ of (a) the BOMEX, SCMS, and ARM cases, and of (b) subsequent stages in the diurnal cycle of the ARM case. The solid line corresponds to the linear fit $\mathcal{N}^*/N = 1.121 - 0.70 \log l$, based on the points with cloud sizes smaller than the scale break size.

The projected cloud fraction decomposition α^p is uniquely determined by the number density $\mathcal{N}$, because it is simply a product of $\mathcal{N}$ and the projected area l^2 [see (4)]. Dividing by the total number of clouds (N) makes the cloud fraction decompositions collapse at the smaller cloud sizes, see Figs. 5a and 5b. The power-law behavior of the densities is even more profound in this figure. The intermediate maximum in α^p is located at the position of the scale break in $\mathcal{N}$. The fact that α^p and $\mathcal{N}$ are so closely related and behave so uniformly in the three simulated cases supports the idea that they can be parameterized by a universal functional form. Knowledge of the position of the scale break and the power-

Unauthenticated | Downloaded 05/26/24 10:08 PM UTC

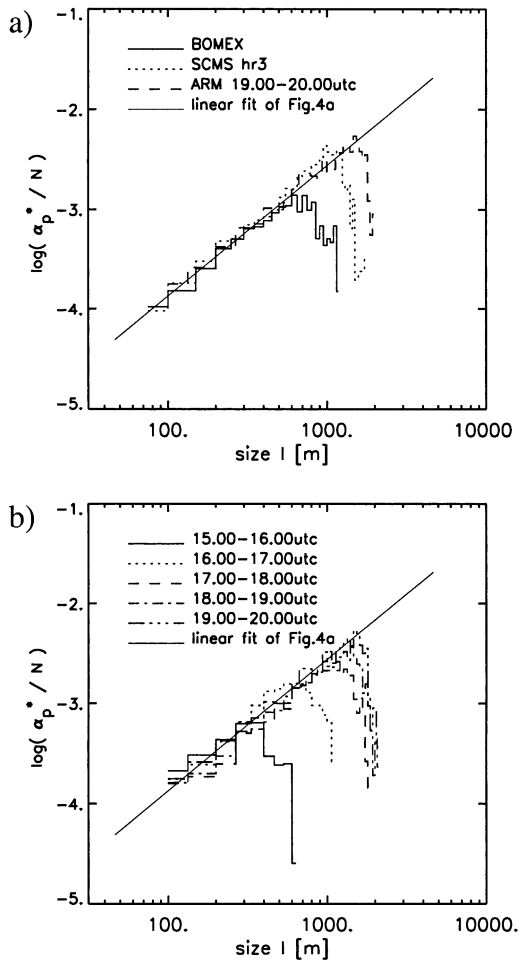

FIG. 5. The normalized projected cloud fraction decomposition α^{p*}/N of (a) the BOMEX, SCMS, and ARM cases, and of (b) subsequent stages in the diurnal cycle of the ARM case. The linear fit corresponding to Fig. 4a using (4) is also plotted as a solid line.

law exponent enables the reproduction of the cloud size density and the projected cloud fraction decomposition, at least for the cloud sizes smaller than the scale break. The power-law exponent seems to be rather robust over all cases, but in contrast the scale break size differs considerably (see Table 2). During the ARM case, the location of the scale break also progresses toward larger sizes with time, reaching a maximum in the afternoon. One might think that the sudden break in the scaling at the larger cloud sizes is a result of insufficient statistics, as the very large clouds seldom occur. However, a convergence test (not shown) made clear that this is not the case: improving the statistical quality of the histogram by increasing the number of sampled clouds does not affect the position of the scale break, nor does the histogram change at the sizes above the break.

These results suggest that the scale break size is the only relevant length scale in the cloud size density. Therefore, we further scale the cloud size densities by nondimensionalizing the cloud size with the scale break

TABLE 2. The position of the scale break in the cloud size densities of the BOMEX, SCMS, and ARM case.

Case	Scale break size (m)
BOMEX	700
SCMS	1050
ARM 1500–1600 UTC	400
ARM 1600–1700 UTC	700
ARM 1700–1800 UTC	1000
ARM 1800–1900 UTC	1100
ARM 1900–2000 UTC	1250

size (see Fig. 6). The data collapse in this figure of all cases over all sizes corroborates the idea of a universal description of the whole cloud size density, also above the scale break. In this region clearly another exponent applies, or perhaps even a totally different functional form. Nevertheless, Fig. 6 illustrates that the scale break size is the only variable. Which mechanism controls the occurrence of the scale break size is a key question that still remains open after this study. The results on the ARM case might suggest that the depth of the (sub)cloud layer plays a role (see also Fig. 2). Cahalan and Joseph (1989) suggested that the scale break size is related to the largest individual convective cells that exist in the boundary layer. Another possible mechanism was discussed by Jonker et al. (1999). In this LES study the important role of (fluctuations in) the specific humidity field was revealed by filtering out the large-scale humidity fluctuations in the subcloud layer. This immediately had a dramatic effect on the typical cloud size of the population.

b. Domination by intermediate sized clouds

Figure 7a shows the same projected cloud fraction decompositions, but now plotted nonnormalized with

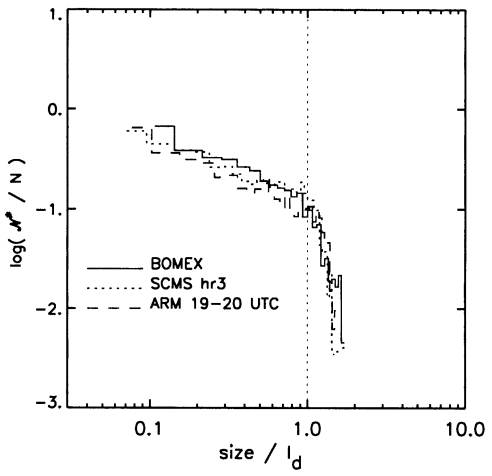

FIG. 6. The normalized cloud size density $\mathcal{N}^*/N$ of the BOMEX, SCMS, and ARM cases. The cloud size ℓ on the horizontal axis is divided by the scale break size ℓ_d. The dotted line marks the scale break.

Unauthenticated | Downloaded 05/26/24 10:08 PM UTC

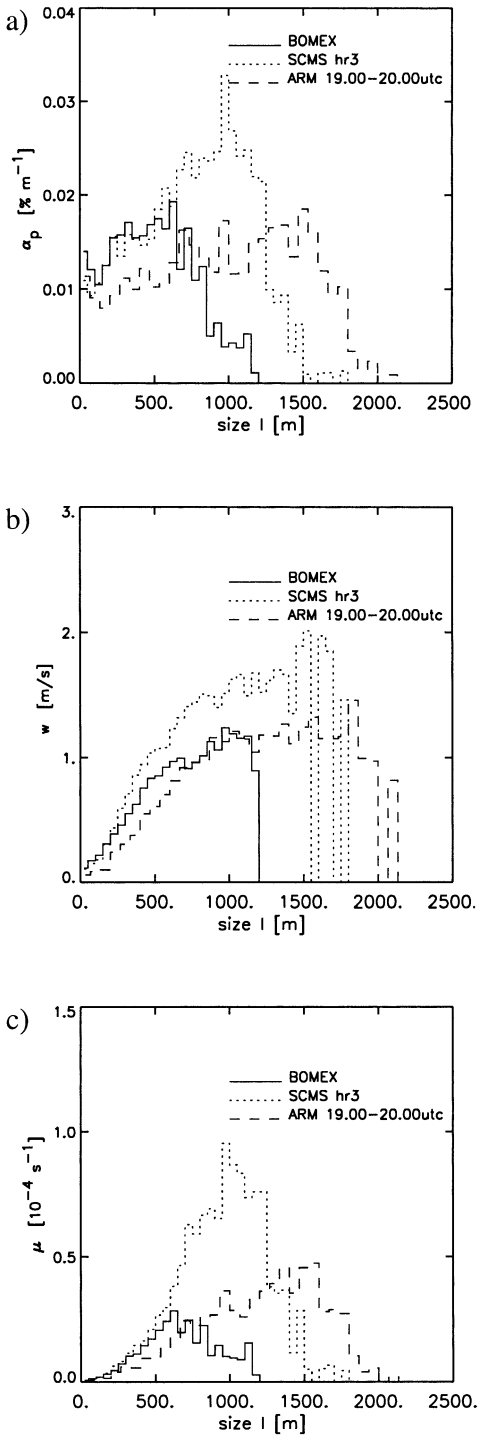

FIG. 7. Cloud size decompositions of the BOMEX, SCMS, and ARM case of (a) the projected cloud fraction α^p and (c) the vertical mass flux μ. (b) The cloud average vertical velocity w as a function of cloud size.

TABLE 3. The total projected cloud cover a^p and the total mass flux m for the BOMEX, SCMS, and ARM case.

Case	a^p (%)	m (m s^{-1})
BOMEX	14.15	0.015
SCMS	26.72	0.060
ARM 1900–2000 UTC	23.27	0.043

linear axes (a common format in many presentations of observational results). The total projected cloud fraction a^p in each case is the surface covered by the histogram (see Table 3). Also in this figure the clouds of an intermediate size contribute most to a^p in all three cases. The fact that the dominating size is intermediate results from the existence of the scale break in $\mathcal{N}$, which is closely related to α^p [see (4)]. If $\mathcal{N}$ were a simple power law with exponent b without a scale break, then

$$\alpha^p(l) \sim l^{(b+2)} \rightarrow \begin{cases} b < -2 & \text{domination by the smallest clouds} \\ b > -2 & \text{domination by the largest clouds.} \end{cases} \tag{10}$$

Instead, in accordance with observations we do find a scale break, with $b = -1.70$ below and $b < -2$ above the scale break size. This implies that $\alpha^p(l)$ increases with l below the scale break and decreases above it: hence a dominating size that is intermediate. Again this shows that the existence of the scale break in $\mathcal{N}$ is essential for the presence of an intermediate dominating size in α^p. Knowledge of the position of the scale break directly gives the dominating size in the projected cloud fraction and vice versa. This intermediate dominating size is also typically found in the projected cloud fraction decomposition of real shallow cumulus cloud fields (Plank 1969; Wielicki and Welch 1986). It illustrates that LES resolves a cloud population with characteristics comparable to nature. The one-gridbox clouds in LES seem to cover somewhat too much area as would be expected from these observations, which typically show α^p to be converging to zero for the smallest clouds. This is probably caused by the numerics of the model (see next section).

In the mass flux decomposition $\mu(l)$, as shown in Fig. 7c, the dominating size is even better defined, although shifted somewhat toward the larger sizes compared to the projected cloud fraction decomposition. This results from the fact that the mass flux is the product of the projected cloud fraction and the cloud-average vertical velocity (see Fig. 7b). The smallest clouds in the spectrum contribute close to nothing to the vertical transport, mainly because of their very low vertical velocities.

More insight in the role of the smallest clouds may be obtained from Fig. 8. It shows the vertical profiles of the contribution of clouds larger than a certain size to the cloud fraction $a(z)$ and the related mass flux $m(z)$. At cloud base ($z = 600$ m) the clouds smaller than 200 m indeed contribute the most. At greater heights, the

Unauthenticated | Downloaded 05/26/24 10:08 PM UTC

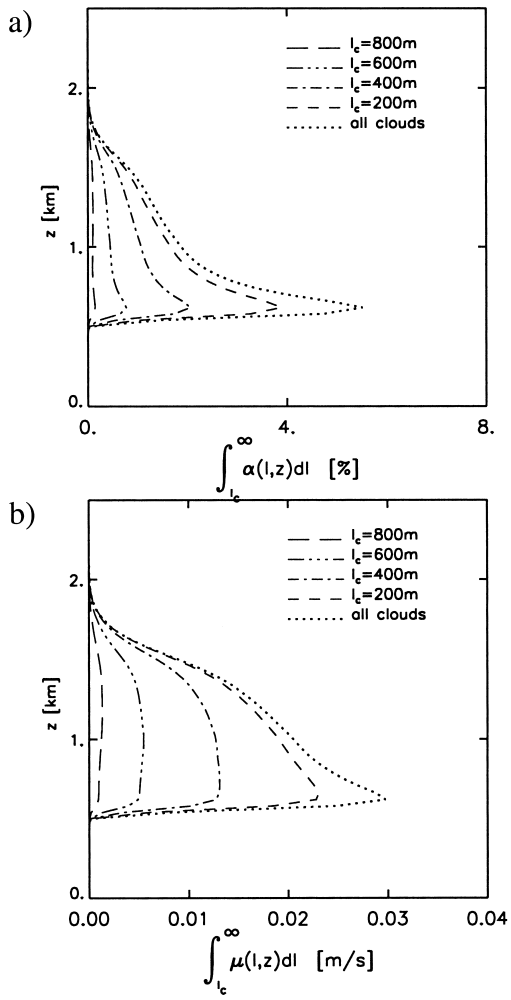

FIG. 8. Vertical profiles of the cumulative cloud size decompositions of (a) cloud fraction $\alpha(l, z)$ and (b) mass flux $\mu(l, z)$. The cumulative decomposition is the sum of all bins of the sizes larger than a certain value l_c, as indicated in the legend.

larger clouds become much more important. This reflects the presence of the numerous small clouds near cloud base, which do not rise very far into the cloud layer. The smallest clouds contribute very little to the mass flux, except at cloud base where their large number somewhat compensates their low vertical velocities. The largest clouds even show a slightly increasing mass flux with height, due to their approximately constant fraction (see Fig. 8a) and increasing vertical velocity with height.

c. Sensitivity to resolution

The results discussed previously in this section were obtained with simulations using only one particular numerical configuration. Therefore, several aspects of the numerics are altered to investigate whether or not the size distributions are robust with respect to changes in discretization. First, the influence of the horizontal grid spacing is studied by performing additional runs with horizontal grid spacings of 25 and 100 m, retaining the domain size. Figure 9a illustrates that the smallest clouds are always the most numerous. The scaling seems to continue at ever smaller sizes, which further supports the use of the power-law function for the cloud size density below the scale break. Nevertheless, at least one extra order of magnitude of small cloud sizes is needed to get some certainty about this. This would require a grid spacing of about 1 or 2 m in LES, a resolution that is expected to be manageable in the near future.

With decreasing grid spacing each one-gridbox cloud also contributes less to the total cloud fraction because its area is smaller. This counteracts the observed increasing number of smallest clouds. A priori it is not known which of these two processes dominates or, in other words, if the cloud fraction decomposition converges to small values for the smallest clouds with increasing resolution. Figure 9b illustrates that α^p converges toward zero at the smallest cloud size with increasing resolution. As a consequence, the intermediate dominating size becomes better defined. But the most important thing is that its intermediate position as well as its amplitude are invariant in this range of grid spacings. Even in the simulation with the very coarse grid spacing of 100 m, which is close to the dominating size in the cloud fraction and which is also used in the GCSS case of BOMEX (Siebesma et al. 2003), the dominating clouds have the same size. Also note that the largest cloud size produced by LES is robust in this range of resolutions. In general the conclusion is that the shape of the cloud fraction decomposition is unaffected by changes of grid spacings in this range.

Table 4 shows that the changes in the projected cloud fraction and in the maximum cloud fraction at any level in the cloud layer are not systematical. However, the total cloud mass flux seems to increase with improving resolution. A smaller grid spacing makes the LES model resolve the dynamics on increasingly smaller scales, but note that the smallest clouds are not responsible for the increase in mass flux: the largest differences are caused by the clouds of sizes equal to the dominating size or larger. The histogram of $\Delta x = 25$ m in Figs. 9b and 9c clearly is not smooth and shows significant peaks at the largest sizes. Larger clouds occur less frequently, and when the period of averaging is too short this causes scatter in the cloud size density, which increases with cloud size. Only a few high-resolution runs could be performed due to limited available CPU simulation time. Furthermore, the impact of this increasing scatter with size in the cloud size density on the decompositions of the cloud fraction and mass flux is further amplified by the fact that larger clouds also cover a larger area individually. To summarize, the impact of scatter caused by bad statistics increases with cloud size. This is clearly visible in Figs. 9b and 9c. The increase in mass flux is therefore likely a result of deteriorating statistics at the largest cloud sizes with improving resolution.

Unauthenticated | Downloaded 05/26/24 10:08 PM UTC

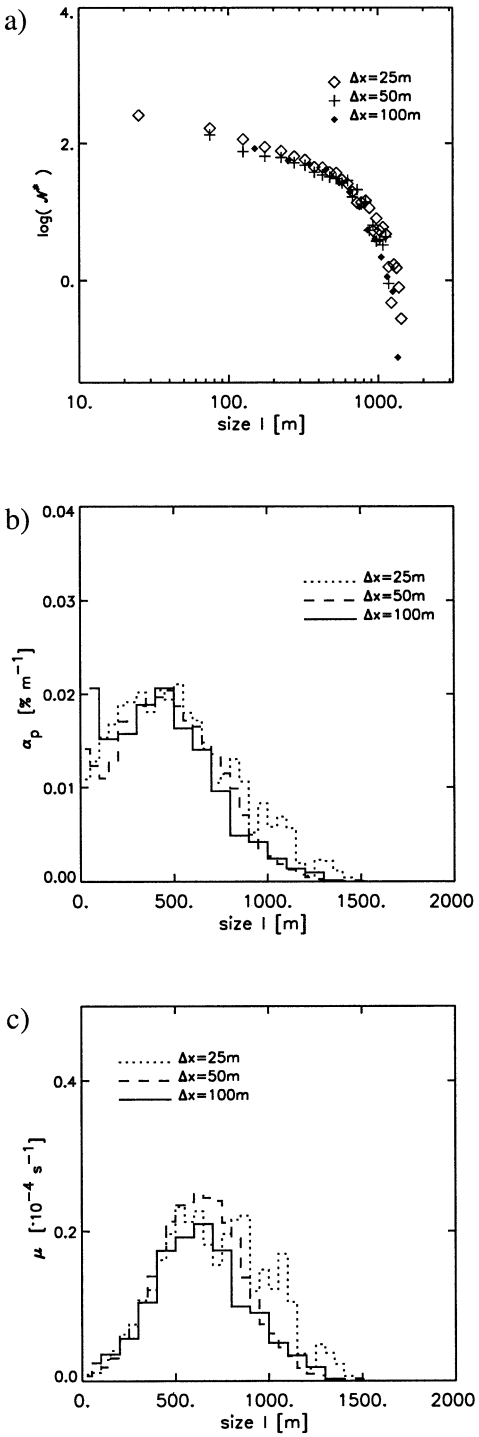

FIG. 9. The (a) cloud size densities $\mathcal{N}^*$ and the size decompositions of (b) the projected cloud fraction α^p and (c) the mass flux μ for LES runs of the BOMEX case with horizontal grid distances of 25, 50, and 100 m.

TABLE 4. The total projected cloud fraction a^p, the maximum cloud fraction a^{max} in the cloud layer, their ratio, and the total mass flux m for several BOMEX simulations. The first three simulations had a different horizontal resolution, the last three had a varying wind shear.

Specifics of simulation	a^p (%)	a^{max}(%)	$\frac{a^p}{a^{max}}$	m (m s^{-1})
Δx = 100 m	14.48	5.85	2.48	0.0127
Δx = 50 m	14.15	5.57	2.54	0.0145
Δx = 25 m	16.41	6.12	2.68	0.0162
0× shear	13.04	6.58	1.98	0.0145
1× shear	14.15	5.57	2.54	0.0145
2× shear	19.38	6.36	3.04	0.0149

d. *Sensitivity to domain size*

Another numerical aspect that may affect the size densities is the dimension of the simulated domain. Three simulations are performed using the SCMS conditions, their horizontal domain sizes being 3.2, 6.4, and 12.8 km. The number of grid boxes in the horizontal was kept constant at 128 × 128. This means that the resolution decreases with increasing domain size, but from Fig. 9 we conclude that the potential effect of the domain size on the densities probably overwhelms those of the resolution. The cloud size decompositions in Fig. 10 illustrate that the largest clouds of the undisturbed 12.8-km domain run are missing in the spectrum of the 3.2-km run, which indicates that the growth of the largest cloud size with time is already limited by this very small domain size in the third hour of simulation. Also, the dominating sizes in the projected cloud fraction and mass flux decompositions have shifted to the largest cloud size. We may conclude that the individual clouds that make up the population are seriously affected if the domain size is chosen too small.

e. *Effects of vertical wind shear*

Vertical shear of the horizontal wind in the cloud layer may influence the position of the dominating size in the size decompositions, as tilting of clouds increases their projected area. Several runs are performed using the BOMEX basic setup with an altered wind shear over the boundary layer, from zero to twice the standard BOMEX initial wind profile. As may be expected, enhancing the tilting of clouds with height by intensifying the wind shear increases the projected size of a cloud and therefore broadens the cloud size density (see Fig. 11a). As a result, the total projected cloud fraction gets larger (see Table 4). This is in agreement with the results of the study on the effects of shear by Brown (1999a). Note that the changes in total cloud fraction by shear are significantly larger than the impact of changes in resolution in these ranges Brown (1999a) reported a shift of the cloud size density to smaller cloud sizes with increasing resolution. The heights of the clouds were not affected, which means that the aspect ratio of cloud width over depth is smaller, implying less cloud

Unauthenticated | Downloaded 05/26/24 10:08 PM UTC

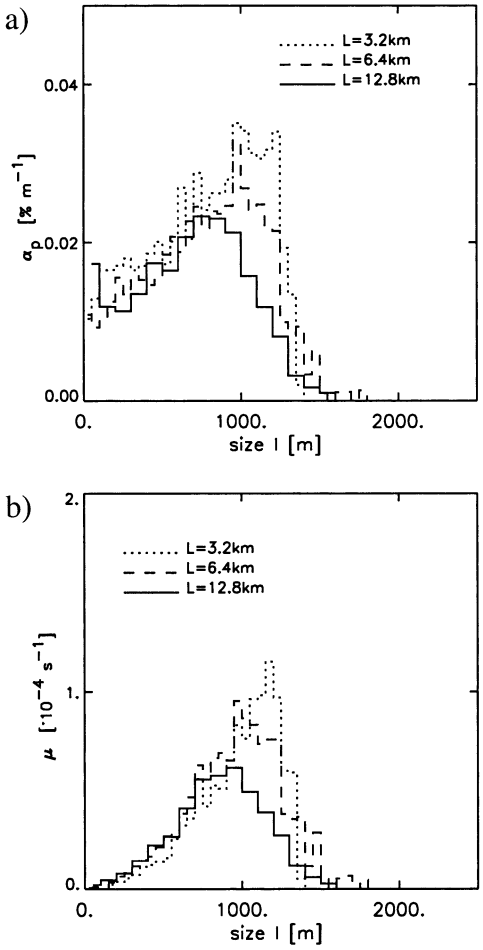

FIG. 10. The cloud size decompositions of (a) the projected cloud fraction α^p and (b) the mass flux μ for three LES runs of the SCMS case with horizontal domain sizes of 3.2, 6.4, and 12.8 km, averaged over the 3D hour of simulation.

overlap. This would make the cloud fraction decomposition more sensitive to wind shear. However, we cannot observe such a shift to the smaller sizes with increasing resolution (see Fig. 9a), and based on this result we do not expect that the impact of shear is dependent on the resolution.

Figure 11a illustrates that the position of the scale break is quite dependent on the intensity of the wind shear. As a consequence, the closely related intermediate dominating size in the projected cloud fraction and mass flux decompositions also changes (see Figs. 11b and 11c). This increasing scale break size is caused by the tilting of the clouds: the change of the maximum cloud size is approximately proportional to the change of the scale break size. The existence of the scale break itself is controlled by something else, as discussed earlier. The presence of wind shear in the cloud layer only complicates the relation between the exact scale break size and the process that determines its occurrence in the first place, such as perhaps the boundary layer height.

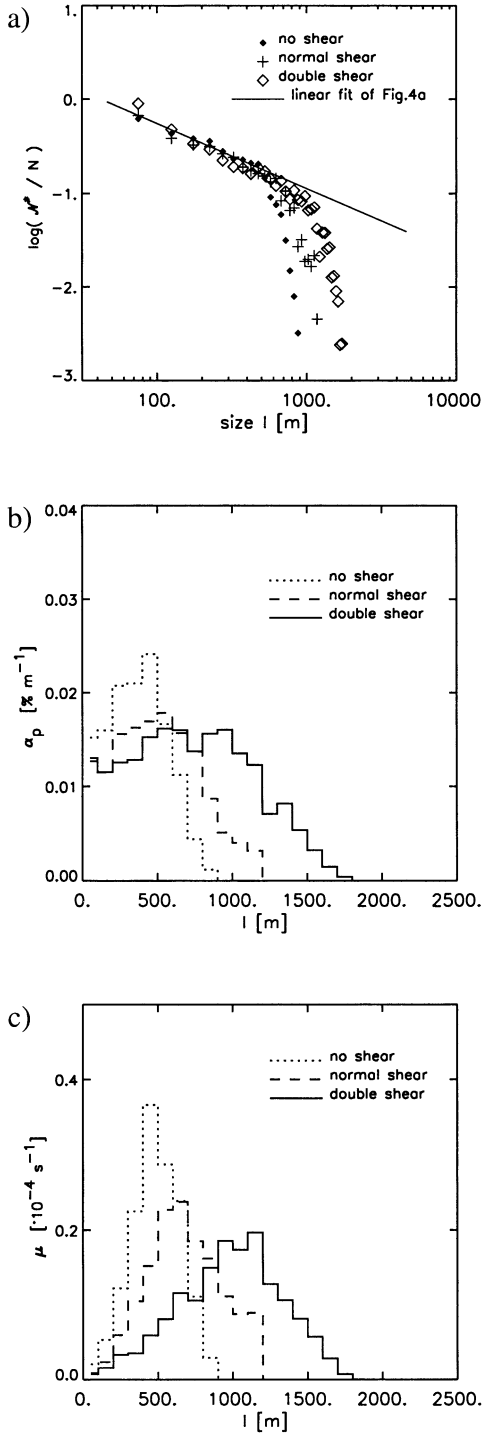

FIG. 11. The cloud size densities and decompositions of three different LES runs of the BOMEX case, in which the initial profile of the horizontal wind is multiplied by 0, 1, and 2 at all levels, respectively. (a) The normalized cloud size densities $\mathcal{N}^*/N$. (b) and (c) The size decompositions of the projected cloud fraction a^p and the mass flux μ. The linear fit of Fig. 4a is also plotted in (a) as a solid line.

Unauthenticated | Downloaded 05/26/24 10:08 PM UTC

While the geometry of the individual clouds is affected by the wind shear, the total vertical mass flux remains approximately constant in all cases (see the area under the histograms in Fig. 11c and Table 4). The vertical turbulent mixing by the clouds tends to destroy the conditional instability in the cloud layer. This is not altered by a different wind shear. The shape of the clouds itself may change by increasing the shear, but the total vertical transport associated with the cloud fields remains the same.

f. Comparison to another LES study

Brown (1999b) reported cloud size decompositions in LES, which shifted to smaller sizes by increasing the horizontal resolution. This is in sharp contrast with the results presented here, in which no shifting takes place: the dominating size is robust and the largest cloud sizes are found to be insensitive to resolution. What is the explanation for these differences? Note that the methods differ at two major points. First, Brown (1999b) derived cloud fraction decompositions *at one level*, while we compute *projected* cloud fraction decompositions. Second, he calculated cloud sizes from the cross-sectional areas of the clouds at that particular height, while in this analysis each cloud has one size, namely, the square root of its vertically projected area (see Fig. 3). The vertical projected area of a cloud takes into account the tilting of clouds by horizontal wind shear and also the typical heterogeneity of the cumulus cloud boundary (Lovejoy 1982; Cahalan and Joseph 1989; Benner and Curry 1998; Siebesma and Jonker 2000). This method is exactly the same as used in satellite image analyses, and is chosen here to enable a straightforward comparison between the LES results and these observational results.

In order to compare our results with the results of Brown (1999b), we also applied the method he used to the cloud fields as produced by our model. One particular level in the cloud layer in BOMEX is chosen for evaluation, at $z = 900$ m. Figure 12a illustrates that the cloud size densities produced by the two different methods are very different: when using the projected cloud area, more small clouds and larger cloud sizes are obtained, and the cloud size density decays more rapidly with cloud size. Small clouds can exist at all levels in the cloud layer, while the largest clouds typically can be as deep as the cloud layer itself. Therefore, when vertically projecting the cloud fractions at all heights ''onto'' one projected cloud fraction, the number of smaller clouds becomes very large. This results in the typical negative power-law exponent in the cloud size density as found for projected cloud fields. Figure 12b shows the cloud fraction decompositions at $z = 900$ m using the method of Brown (1999b). It is clear that this decomposition also does not shift to smaller sizes when the horizontal resolution of the simulations is increased:

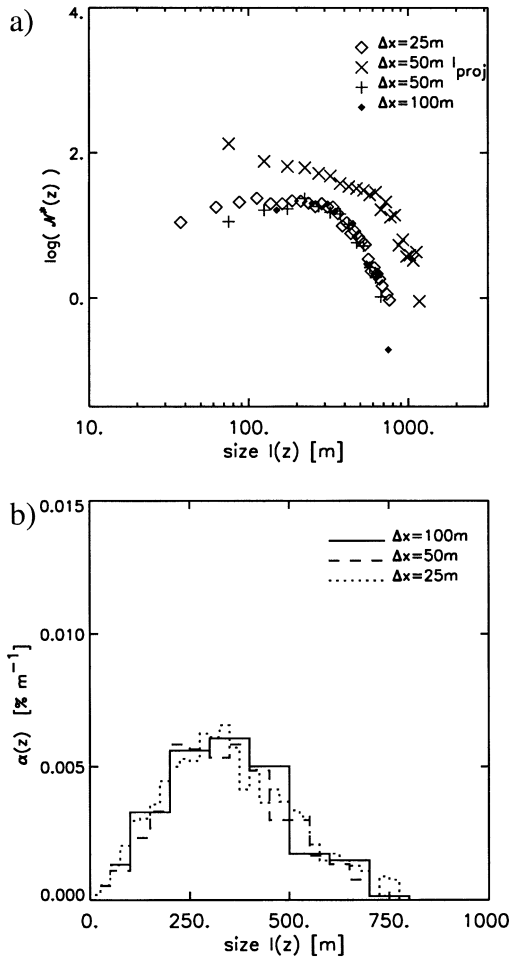

FIG. 12. The (a) cloud size density $\mathcal{N}^*$ and (b) the cloud fraction decomposition α^p at $z = 900$ m for the BOMEX case for three different horizontal resolutions. The cloud sizes $l(z)$ were calculated from the cross-sectional areas of the clouds at that level. The cloud size density of Fig. 9a with $\Delta x = 50$ m is also plotted for comparison.

the maximum cloud size as well as the intermediate dominating size are robust in this range of resolutions.

The remarkable different behavior of the cloud size densities in these two LES studies may be due to different statistics. Many subsequent cloud fields are needed to sample the clouds with largest sizes and timescales sufficiently. The histograms in this LES study are always based on about 10^4 clouds or more, which is a number typically captured by high-resolution satellite images. The cloud size densities presented earlier in this paper are calculated with the same method as applied in many observational studies, and we found their power-law exponent and scale break to be realistic. This gives us confidence in the statistical quality of the histograms as presented here.

Another explanation for the different sensitivity to horizontal resolution can be the use of different types of subgrid-scale (SGS) models. The SGS model plays a significant role in the mixing processes between the

Unauthenticated | Downloaded 05/26/24 10:08 PM UTC

clouds and their environment, and might therefore have an impact on the cloud size density. The KNMI LES model uses a prognostic subgrid turbulent kinetic energy (TKE) equation, while a version of the Smagorinsky model is applied in the LES model of Brown (1999b). Stevens et al. (1999) reported that in smoke cloud simulations the use of a Smagorinsky-type SGS model results in a much higher sensitivity of the entrainment fluxes to the effective resolution when compared to a prognostic TKE SGS model. This is due to the capacity of the latter model to compensate the SGS eddy viscosity for changes that lead to a smaller resolved entrainment flux, because the same changes simultaneously enhance the buoyant production of subgrid TKE. This feedback mechanism may also apply to the SGS and resolved entrainment into simulated cumulus clouds, and can therefore be responsible for the observed smaller sensitivity in the KNMI LES model to horizontal resolution. These issues need to be investigated in more detail in future studies.

5. Discussion and conclusions

The main conclusion of this study is that the shallow cumulus cloud populations produced by LES match natural populations at several important points. The simulated cloud size density is well described by a power law for the smaller clouds, with an exponent of -1.70. The scaling breaks down at a certain cloud size, above which the number density quickly falls off. The sensitivity test for the horizontal resolution suggests that this scaling continues at sizes smaller than the typical grid spacing of present-day LES, although at least one extra order of magnitude of cloud sizes is needed to actually prove this. These LES results strongly support the power laws and scale breaks observed by Cahalan and Joseph (1989), Kuo et al. (1993), and Benner and Curry (1998), and give no evidence for the exponential function (Wielicki and Welch 1986) or the lognormal function (Lopez 1977). In conclusion, the observed power law for the smaller cumulus cloud populations appears to be an important and robust geometrical fingerprint. Therefore, a quantitative physical explanation for this behavior is an outstanding scientific challenge that remains to be resolved.

The projected cloud fraction decomposition is uniquely determined by the cloud size density. The existence of the scale break, combined with the typical power-law exponent for the smaller clouds, causes a well-defined, intermediate dominating size in both the projected cloud fraction and mass flux decompositions. This is consistent with cloud fraction decompositions of observed cloud populations. The cloud size densities show a remarkable uniformity over the three simulated cases. This feature facilitates the parameterization of these cloud size densities and decompositions. The only variable is the position of the scale break, and with it the dominating size. Which process actually controls the scale break size remains unclear and is not answered in this study, although we have shown that the (sub)cloud-layer height and the intensity of wind shear play a role. Another process that likely affects the size distribution of clouds is the nature of the dry turbulence in the subcloud layer, as most large clouds root in this layer. This would link the scale break size to the cloud–subcloud layer interaction. Perhaps the two distinctly different regimes of the cloud size density above and below the scale break represent two different processes, the one determined by the coherent structures of the subcloud layer turbulence and the other by the decay of the large clouds into smaller ones (the scaling region). It is evident that more thorough research is needed to give insight in this problem. LES would be a suitable numerical laboratory to conduct further research on this subject (e.g., Jonker et al. 1999).

The intermediate position of the dominating cloud size shows that the clouds that are most important for the projected cloud fraction and vertical transport are not of resolution scale but are significantly larger. This is fortunate, for the subgrid model of LES plays an important role in the dynamics of the smallest clouds, while the larger clouds are resolved better by the discretized governing equations. We find here that those larger, better-resolved clouds contribute most to the total projected cloud fraction and mass flux of the population. The smallest clouds contribute close to nothing to the vertical mass transport. This feature is invariant over a range of horizontal resolutions for BOMEX. This point is important for the interpretation of the performance of LES on shallow cumulus in general. Apparently, apart from being robust in producing cloud-field-average statistics, LES is also consistent in producing realistic cloud populations. The exact definition and complete control over all conditions in LES has several important advantages: the possibility of reproducing obtained results for similar settings, and therefore the possibility to carry out systematic impact studies of key parameters in the system. On top of this LES offers almost unparalleled statistical possibilities by performing independent ensemble runs.

Acknowledgments. The LES results in this study were obtained using the supercomputer facilities of the European Centre for Medium-Range Weather Forecasts in Reading, United Kingdom. We acknowledge NCAR and its sponsor the National Science Foundation for the use of the SCMS data, which was provided to us by Peter Duynkerke.[1] Furthermore we thank two anonymous reviewers for their critical but constructive remarks, and Dave Donovan at the KNMI for carefully prereading and correcting the manuscript. This study has been supported by the Netherlands Organization for Scientific Research under Grant 750.198.06.

Unauthenticated | Downloaded 05/26/24 10:08 PM UTC

APPENDIX

Elementary Definitions of Cloud Size Densities

An instantaneous 3D cloud field is denoted by $c(i, j, k, t) \in \{0, 1\}$, (0: noncloudy, 1: cloudy grid box, where cloudy is defined as the grid box being saturated). The indices i, j, k are the 3D coordinates of the grid box, and t marks the time. An offline algorithm determines the number of individual clouds at time t, denoted by $N(t)$. The algorithm creates N fields $c_n(i, j, k, t)\{0, 1\}$, $n = \{1, \ldots, N\}$, which indicate whether or not a grid box belongs to cloud number n. We will omit indication of time hereafter.

The volume of cloud n is

$$V_n = \Delta x \Delta y \Delta z \sum_{ijk} c_n(i, j, k). \tag{A1}$$

The area of cloud n at height $z_k = (k - 1/2)\,\Delta z$ is

$$A_n(z_k) = \Delta x \Delta y \sum_{ij} c_n(i, j, k). \tag{A2}$$

The height averaged area is given by

$$A_n^a = \frac{1}{h_n} \sum_{k=k_{n,\text{base}}}^{k_{n,\text{top}}} A_n(z_k)\Delta z, \tag{A3}$$

where h_n is the height of cloud n

$$h_n = \Delta z[k_{n,\text{top}} - k_{n,\text{base}} + 1]. \tag{A4}$$

The mass flux of cloud n at height z_k is (with $\rho = 1$)

$$M_n(z_k) = \Delta x \Delta y \sum_{ij} c_n(i, j, k) w(i, j, k). \tag{A5}$$

It is useful to define the ''vertically projected'' fields:

$$c_n^p(i, j) = H\left[\sum_k c_n(i, j, k)\right], \tag{A6}$$

where H denotes the Heaviside function. The vertically projected area of cloud n is then

$$A_n^p = \Delta x \Delta y \sum_{ij} c_n^p(i, j). \tag{A7}$$

Each cloud n in the population is given a unique size ℓ_n, as defined in the text. Then, we define the following *set*:

$$I(l) \equiv \{1 \le n \le N | \ell_n < l\}, \tag{A8}$$

that is, $I(l)$ represents the set of clouds that have linear size smaller than a given size ℓ. The number of clouds smaller than ℓ is

$$N(l) = |I(l)|. \tag{A9}$$

Obviously,

$$\lim_{l\to\infty} N(l) = N \qquad \lim_{l\to\infty} I(l) = \{1, \ldots, N\}. \tag{A10}$$

The ''projected'' area of clouds smaller than ℓ is

$$A^p(l) = \sum_{n\in I(l)} A_n^p, \tag{A11}$$

with A_n^p defined by (A7). The mass flux at z_k transported by clouds smaller than ℓ is

$$M(l, z_k) = \sum_{n\in I(l)} M_n(z_k), \tag{A12}$$

where $M_n(z_k)$ is defined in (A5).

Rather than $M(l, z)$ and $A^p(l)$ we are generally more interested in the fractional quantities, such as projected cloud fraction, etc.,

$$m(l, z) \equiv \frac{M(l, z)}{L_x L_y} \qquad a^p(l) \equiv \frac{A^p(l)}{L_x L_y}, \tag{A13}$$

where L_x and L_y refer to the horizontal domain sizes.

The following equations follow directly from the definitions. The total number of clouds, the total projected cloud fraction, and the total fractional mass flux is

$$m(z_k) = (L_x L_y)^{-1} \sum_n M_n(z_k) = \lim_{l\to\infty} m(l, z_k) \tag{A14}$$

$$a^p = (L_x L_y)^{-1} \sum_n A_n^p = \lim_{l\to\infty} a^p(l) \tag{A15}$$

$$N = \lim_{l\to\infty} N(l). \tag{A16}$$

Particularly interesting are the corresponding densities

$$\mathcal{N}(l) \equiv \frac{d}{dl}N(l), \qquad \alpha^p(l) \equiv \frac{d}{dl}a^p(l),$$

$$\mu(l, z_k) \equiv \frac{d}{dl}m(l, z_k), \tag{A17}$$

which permits us to write

$$N = \int_0^\infty \mathcal{N}(l)\, dl, \qquad a^p = \int_0^\infty \alpha^p(l)\, dl,$$

$$m(z_k) = \int_0^\infty \mu(l, z_k)\, dl. \tag{A18}$$

REFERENCES

Arakawa, A., and W. H. Schubert, 1974: Interaction of a cumulus cloud ensemble with the large-scale environment. Part I. *J. Atmos. Sci.,* **31,** 674–701.

Barnes, G. M., J. C. Fankhauser, and W. D. Browning, 1996: Evolution of the mass flux and the diagnosed net lateral mixing in isolated convective clouds. *Mon. Wea. Rev.*, **124,** 2764–2784.

Beniston, M. G., and G. Sommeria, 1981: Use of a detailed planetary boundary layer model for parameterization purposes. *J. Atmos. Sci.*, **38,** 780–797.

Benner, T. C., and J. A. Curry, 1998: Characteristics of small tropical cumulus clouds and their impact on the environment. *J. Geophys. Res.*, **103,** 28 753–28 767.

Brown, A. R., 1999a: Large-eddy simulation and parameterization of the effects of shear on shallow cumulus convection. *Bound.-Layer Meteor.*, **91,** 65–80.

——, 1999b: The sensitivity of large-eddy simulations of shallow cumulus convection to resolution and sub-grid model. *Quart. J. Roy. Meteor. Soc.*, **125,** 469–482.

——, and Coauthors, 2002: Large-eddy simulation of the diurnal cycle of shallow cumulus convection over land. *Quart. J. Roy. Meteor. Soc.*, **128,** 1075–1094.

Unauthenticated | Downloaded 05/26/24 10:08 PM UTC

Cahalan, R. F., and J. H. Joseph, 1989: Fractal statistics of cloud fields. *Mon. Wea. Rev.,* **117,** 261–272.

Cuijpers, J. W. M., and P. G. Duynkerke, 1993: Large-eddy simulation of trade-wind cumulus clouds. *J. Atmos. Sci.,* **50,** 3894–3908.

French, J. R., G. Vali, and R. D. Kelly, 1999: Evolution of small cumulus clouds in Florida: Observations of pulsating growth. *Atmos. Res.,* **52,** 143–165.

Gregory, D., 2001: Estimation of entrainment rate in simple models of convective clouds. *Quart. J. Roy. Meteor. Soc.,* **127,** 53–71.

Holland, J. Z., and E. M. Rasmusson, 1973: Measurement of atmospheric mass, energy and momentum budgets over a 500-kilometer square of tropical ocean. *Mon. Wea. Rev.,* **101,** 44–55.

Jonker, H. J. J., P. G. Duynkerke, and A. P. Siebesma, 1999: Development of mesoscale fluctuations in cloud-topped boundary layers. Preprints, *13th Symp. on boundary Layers and Turbulence,* Dallas, TX, Amer. Meteor. Soc., 197–200.

Kollias, P., B. A. Albrecht, R. Lehrmitte, and A. Savtchenko, 2001: Radar observations of updrafts, downdrafts, and turbulence in fair-weather cumuli. *J. Atmos. Sci.,* **58,** 1750–1766.

Knight, C. A., and L. J. Miller, 1998: Early radar echoes from small, warm cumulus: Bragg and hydrometeor scattering. *J. Atmos. Sci.,* **55,** 2974–2992.

Kuo, K.-S., R. M. Welch, R. C. Weger, M. A. Engelstad, and S. K. Sengupta, 1993: The three-dimensional structure of cumulus clouds over the ocean. I. Structural analysis. *J. Geophys. Res.,* **98,** 20 685–20 711.

Lehrmitte, R., 1987: Small cumuli observed with a 3-mm wavelength Doppler radar. *Geophys. Res. Lett.,* **14,** 707–710.

Lopez, R. E., 1977: The lognormal distribution and cumulus cloud populations. *Mon. Wea. Rev.,* **105,** 865–872.

Lovejoy, S., 1982: Area–perimeter relation for rain and cloud areas. *Science,* **216,** 185–187.

Nitta, T., and S. Esbensen, 1974: Heat and moisture budget analyses using BOMEX data. *Mon. Wea. Rev.,* **102,** 17–28.

Plank, V. G., 1969: The size distributions of cumulus clouds in representative Florida populations. *J. Appl. Meteor.,* **8,** 46–67.

Raga, G. B., J. B. Jensen, and M. B. Baker, 1990: Characteristics of cumulus band clouds off the coast of Hawaii. *J. Atmos. Sci.,* **47,** 338–355.

Siebesma, A. P., and J. W. M. Cuijpers, 1995: Evaluation of parametric assumptions for shallow cumulus convection. *J. Atmos. Sci.,* **52,** 650–666.

——, and H. J. J. Jonker, 2000: Anomalous scaling of cumulus cloud boundaries. *Phys. Rev. Lett.,* **85,** 214–217.

——, and Coauthors, 2003: A large-eddy simulation intercomparison study of shallow cumulus convection. *J. Atmos. Sci.,* in press.

Stevens, B., C.-H. Moeng, and P. P. Sullivan, 1999: Large-eddy simulation of radiatively driven convection: Sensitivities to the representation of small scales. *J. Atmos. Sci.,* **56,** 3963–3984.

——, and Coauthors, 2001: Simulations of trade-wind cumuli under a strong inversion. *J. Atmos. Sci.,* **58,** 1870–1891.

Tiedtke, M., 1989: A comprehensive mass flux scheme for cumulus parameterization in large-scale models. *Mon. Wea. Rev.,* **117,** 1779–1800.

Warner, J., 1970: The microstructure of cumulus cloud. Part III: The nature of the updraft. *J. Atmos. Sci.,* **27,** 682–688.

——, 1977: Time variation of updraft and water content in small cumulus clouds. *J. Atmos. Sci.,* **34,** 1306–1312.

Wielicki, B. A., and R. M. Welch, 1986: Cumulus cloud properties derived using Landsat satellite data. *J. Climate Appl. Meteor.,* **25,** 261–276.

Xu, K.-M., and D. A. Randall, 2001: Updraft and downdraft statistics of simulated tropical and midlatitude cumulus convection. *J. Atmos. Sci.,* **58,** 1630–1649.

Unauthenticated | Downloaded 05/26/24 10:08 PM UTC